Biogeochemistry **48:** 217–235, 2000.

Redox processes in recent sediments of the river Meuse, The Netherlands

GERARD A. VAN DEN BERG[1,*], J.P. GUSTAV LOCH[1], LAMBERTUS M. VAN DER HEIJDT[2] & JOHN J.G. ZWOLSMAN[2]

[1]*Department of Geochemistry, Faculty of Earth Sciences, Utrecht University, PO Box 80.021, 3508 TA Utrecht, The Netherlands;* [2]*Ministry of Transport, Public Works and Water Management, Institute for Inland Water Management and Waste Water Treatment (RIZA), Van Leeuwenhoekweg 20, 3316 AV Dordrecht, The Netherlands (*Present address: Ministry of Transport, Public Works and Water Management, Institute for Inland Water Management and Waste Water Treatment (RIZA), Van Leeuwenhoekweg 20, 3316 AV Dordrecht, The Netherlands)*

Received 26 February 1999; accepted 11 March 1999

Key words: diagenesis, modelling, organic matter, pore water, redox, sediment

Abstract. Pore-water concentrations of inorganic solutes were measured at four locations in a recent sedimentation area of the river Meuse in The Netherlands. The pore-water concentration profiles were interpreted using the steady state one-dimensional reaction/transport model STEADYSED1. This model explicitly accounts for the organic matter degradation pathways and secondary redox reactions. Results show that the model reproduces the measured pore-water profiles of redox species reasonably well, although significant divergence is observed for pH. The latter is due to the absence of pH buffering by $CaCO_3$ in the model. At all locations, methanogenesis is the major pathway of organic matter degradation below 3 cm from the sediment-water interface. However, organic matter degradation rates by methanogenesis may be overestimated, because methane ebullition is not included. Differences in profiles of redox-sensitive ions among the four locations are explained by differences in depositional conditions, in particular the sediment accumulation rate and supply of organic matter.

Introduction

Pore-water distributions of redox-sensitive ions provide considerable information about pathways and rates of organic matter (OM) degradation, and the intensities of physical, chemical and biological processes in sediments (Berner 1980; Santschi et al. 1990). The relative contributions of the microbial pathways of OM mineralisation depend on the flux of OM to the sediment, the biological reactivity of the OM, the availability of electron acceptors, the kinetics of secondary reactions as well as the transport rates. High deposition fluxes of degradable OM in many freshwater systems result

in compressed redox zones, with sulphate reduction occurring within the upper few centimetres of the sediments (Wersin et al. 1991). Because of the limited supply of sulphate, methanogenesis may be an important pathway of OM degradation in freshwater sediments (Capone & Kiene 1988).

Sediments are important sources or sinks of heavy metals in aquatic systems (e.g. Calmano et al. 1993; Gaillard et al. 1986). Because the behaviour of heavy metals in sediments is to a large extent controlled by the redox cycles of the major biogeochemical elements (Shaw et al. 1990), the latter need to be quantified in order to provide a rational basis for managing contaminated water systems (Förstner et al. 1994). Reactive transport models, e.g. Rabouille and Gaillard (1991), Dhakar and Burdige (1996), Soetaert et al. (1996), and Van Cappellen and Wang (1996), have been developed to identify environmental and biogeochemical factors controlling the chemical dynamics of sediments and to predict the behaviour and speciation of redox-sensitive ions. These models were primarily developed to quantify processes in marine systems. The latter model was also tested on freshwater systems (Van Cappellen & Wang 1995).

The purpose of this research is to study redox processes in organic-rich freshwater sediments. Pore water concentration profiles of redox-sensitive ions were measured from sediment cores, taken in a recent sedimentation area of the river Meuse in The Netherlands. The one-dimensional reaction/transport model STEADYSED1 (Van Cappellen & Wang 1996) was used to simulate concentration profiles in order to distinguish between chemical, biological and physical processes, and to show the relative importance and magnitude of redox cycles. This model explicitly accounts for the oxic, suboxic and anoxic OM degradation pathways, and it incorporates the secondary reactions involving the byproducts of OM biodegradation.

Sampling and analysis

Study area

The Biesbosch is a wetland, situated in the delta of the rivers Rhine and Meuse in the western part of The Netherlands (Figure 1). The study area is almost exclusively flushed by the river Meuse, except for its north-western part, where Rhine water occasionally intrudes. Tidal influences in the Biesbosch have decreased considerably after 1970, when the former Rhine-Meuse estuary was closed off from the North Sea by a dam. Today, the Biesbosch is a freshwater tidal basin with a modest tidal range (20–30 cm in the study area). Due to the low current velocities, the former tidal channels are silting up. Both the sediments and soils in the Biesbosch are strongly

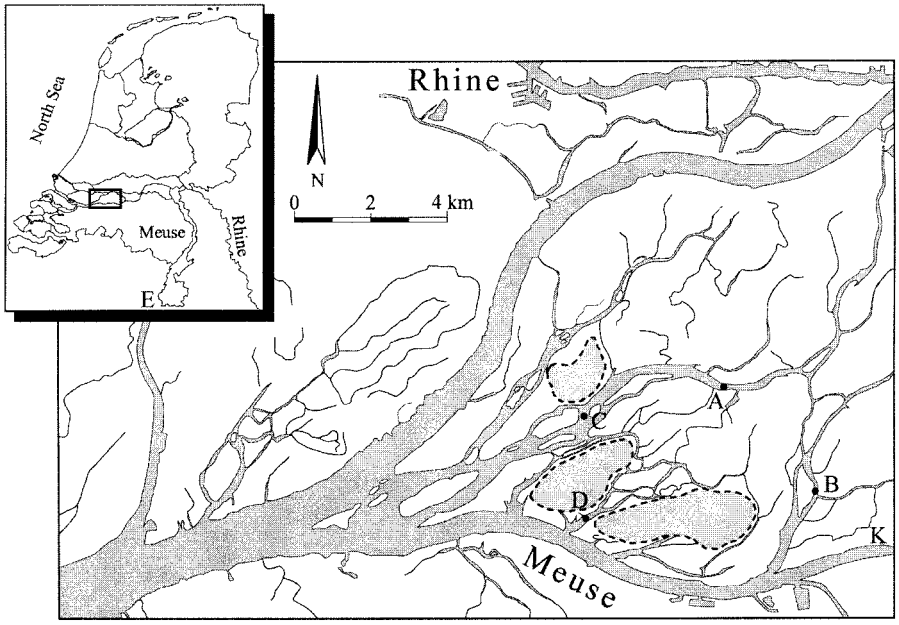

Figure 1. Map of the sampling locations in the Biesbosch. The small map shows The Netherlands and the study area.

contaminated by heavy metals, reflecting the serious metal pollution history of the rivers Meuse and Rhine (Van Eck et al. 1997).

Sample collection and handling

At four permanently submerged locations in the Biesbosch (Figure 1), sediment cores were collected in Plexiglas tubes with an inner diameter of 15 cm and a length of 60 cm. This broad diameter was chosen in order to minimise sediment disturbance during sampling. Mean water depth at the locations A, B, C, and D is 1.4, 2.0, 4.2, and 3.3 m, respectively. Sampling took place manually by SCUBA divers. In this paper only the results of the sampling campaign in June are discussed. Bottom water remained on the sediment in the tubes to prevent oxidation of the sediment by atmospheric oxygen. The collected cores were tightly sealed and stored at 4 °C. Pore-water pH was measured on board with a MI-410/MI-415 pH micro-electrode (Microelectrode INC.) equipped with a micro-manipulator. To avoid disturbance of the sediment, pH measurements were conducted in a second core with similar solid-phase characteristics as the one used for pore-water and solid-phase extractions. Bottom water was sampled at the same locations at 0.5 m above the sediment-water interface (Table 1). Collected bottom water was

Table 1. Characteristics of the bottom water, collected in June 1996 at a depth of 50cm above the sediment-water interface.

	Unit	Range	Mean value
Temperature	°C	21.1–22.4	21.7
Salinity	‰	0.25–0.27	0.26
pH	–	7.6–8.6	8.0
Cl^-	mmol l^{-1}	2.02–2.21	2.14
O_2	mmol l^{-1}	0.24–0.55	0.36
NO_3^-	mmol l^{-1}	0.15–0.25	0.21
Mn^{2+}	μmol l^{-1}	<0.05	<0.05
Fe^{2+}	μmol l^{-1}	<0.11	<0.11
SO_4^{2-}	mmol l^{-1}	0.65–0.69	0.67
Alkalinity	$mmol_c$ l^{-1}	3.64–3.87	3.80
NH_4^+	mmol l^{-1}	<0.01	<0.01

filtered through a 0.45 μm membrane filter (Sartorius). Suspended matter was collected by continuous flow-through centrifugation.

Within 24 h (cores A, B and C) and 48 h (core D) after collection, the top 7 cm of the sediment cores were sectioned into 0.5- or 1.0-cm slices and pore-water extraction took place. Laboratory sampling took place under strictly anaerobic conditions in a nitrogen-filled glove box. Pore water was extracted by pressure filtration, according to the method described by De Lange (1992), and collected in High Density Polyethylene bottles. Part of the pore water was acidified with concentrated suprapur HNO_3 (1 ml HNO_3 per 50 ml pore water). Sediment and nonacidified pore-water samples were kept at 4 °C under a nitrogen atmosphere until extraction and analysis. All materials (bottles, filters, and filtration blocks) were acid-cleaned prior to use.

Sediment and pore-water analysis

Freeze-dried sediment samples were digested in a mixture of concentrated $HClO_4$, HNO_3 and HF and finally dissolved in 1 M HCl. Elemental concentrations in the acid solution were determined by inductively coupled plasma atomic emission spectrometer (Perkin Elmer Optima 3000). The quality of the analyses was tested by simultaneously extracting and analysing international standard sediments. Accuracy was within 5% of the tabulated concentrations for all elements of interest. Measurement of organic C (C_{org}) and total N (N_{tot}) contents in sediment and suspended matter was made with

a CNS analyser (Carlo Erba Strumentazione nitrogen analyzer 1500). Inorganic carbon was removed before analysis by shaking the sediment sample in 1 M HCl. ^{210}Pb activity was measured indirectly by alpha-spectrometry of its daughter product ^{210}Po on dried sediment samples from location C. Moisture content of the sediment samples, necessary to calculate porosity, was determined by measuring the weight loss after freeze drying.

Collected bottom waters were analysed on board for temperature, dissolved oxygen, pH, and salinity. Shipboard measurements took place with a sensor system. Pore waters and bottom waters were analysed for concentrations of major elements (e.g. Mn, Fe, and Ca) by ICP-AES. Ammonium was determined spectrophotometrically by means of a modified Berthelot reaction (Solorzano 1969). Sulphate, nitrate and chloride were measured in non acidified surface and pore water by ion-chromatography (Dionex QIC analyser). Alkalinity was determined by the Gran plot method after titration with 0.01 M HCl (Stumm & Morgan 1996).

Early diagenetic model

Model description

The multicomponent reaction/transport model STEADYSED1 (Van Cappellen & Wang 1996) includes kinetic expressions describing decomposition of OM via oxic respiration, denitrification, Mn(IV) reduction, Fe(III) reduction, sulphate reduction, and methanogenesis. Solutes may participate in secondary redox reactions, adsorb on sediment particles or precipitate as authigenic solid phases, like (hydr)oxides, Mn- and Fe carbonates, and sulphides. The model includes solute transport by molecular diffusion, pore-water irrigation, particle mixing, and advective sediment burial. The most important assumption of the model is that geochemical conditions in sediments are at steady-state.

Model parameters are divided into site-specific (environmental) parameters and reaction-specific parameters (Wang & Van Cappellen 1996). The depositional environment is characterised by site-specific parameters, which include sediment accumulation rate, bottom-water chemistry, particulate deposition fluxes, intensities of particle mixing and irrigation, and physical characteristics such as temperature, porosity and particle densities. The chemical transformation processes in the sediment are described by reaction-specific parameters, which include reaction rate coefficients, apparent equilibrium constants, surface-site densities and limiting concentrations of electron acceptors. Secondary redox reactions are described by bimolecular reaction rate laws. Precipitation and dissolution rates are

assumed to depend linearly on the degree of saturation of the pore water with respect to the minerals. The mass conservation equations are solved numerically by finite difference.

Critical parameters in the computation are a set of limiting concentrations for the terminal electron acceptors of the respiratory pathways. These concentrations account for the effects of substrate limitation, inhibition, and competition (Rabouille & Gaillard 1991; Van Cappellen & Gaillard 1996). Respiratory transformation rates are based on a modified Monod formulation (see Van Cappellen & Wang 1996 for further details).

Pore-water modelling approach

Predicted profiles of solute concentrations are calculated by STEADYSED1 using the parameters listed in Table 2. The actual fitting parameters are the deposition rate, OM degradation rate and ammonium concentration in bottom water. Fluxes of reactive Mn- and Fe-(hydr)oxides to the sediment are based on these deposition rates and measured solid-phase levels of Fe and Mn at the sediment-water interface. It is further assumed that 40% of the Fe flux to the sediment consists of reactive Fe(III)(oxyhydr)oxides and the total Mn flux consists of reactive Mn(IV)oxide (Van den Berg 1998). The remainder of the Fe flux is incorporated in the mineral structure of, e.g., clay minerals and relatively unreactive oxides.

Solute transport within the top layer of the sediment takes place by advection, molecular diffusion, bioirrigation and bioturbation. The effects of infiltration are not considered. In many freshwater sediments, especially in dynamic tidal systems, bioturbation dominates transport in the top layer of the sediment, unless anoxic or suboxic conditions prevail in the bottom water. The intensity of biological mixing is influenced by the bottom-water oxygenation and the supply rate of detrital matter. In the top 15 cm of the core at location C, a constant ^{210}Pb activity is measured, which indicates that this layer is most likely subject to intense mixing. A constant (biological) mixing coefficient (D_{mix}) in the top 15 cm of the sediment is assigned to each location. It is assumed that below this depth no significant mixing takes place. Values of the mixing coefficient are calculated using the empirical equation of Tromp et al. (1995), which correlates the amount of (biological) mixing in sediments accumulating in oxic bottom water with the deposition rate

$$\log D_{bio} = 1.63 + 0.85 \log \omega,$$

in which D_{bio} is the (biological) mixing coefficient (in cm^2 yr^{-1}) and ω is the deposition rate (in cm yr^{-1}). The estimated deposition rates reported in Table 2 agree well with those based on sediment fluxes in the study area (RIZA,

Table 2. List of input parameter values.

	Unit	A	B	C	D
Temperature	°C	21.7	21.7	21.7	21.7
Salinity	‰	0.26	0.26	0.26	0.26
Deposition rate	cm yr^{-1}	6	0.3	1	5
Porosity	–	0.86	0.73	0.83	0.83
Particle dry density	g cm^{-3}	2.4	2.4	2.4	2.4
Particle-mixing coefficient	cm^2 yr^{-1}	195	15	42	168
Depth of mixed layer	cm	15	15	15	15
C degradation rate at x = 0	μmol cm^{-3} yr^{-1}	600	150	150	950
Depth-attenuation coefficient	cm^{-1}	0.15	0.32	0.15	0.25
Molar C:N:P ratio	–	20:1.6:1	20:1.6:1	20:1.6:1	20:1.6:1
Flux MnO_2	μmol cm^{-2} yr^{-1}	60	3	10	50
Flux $Fe(OH)_3$	μmol cm^{-2} yr^{-1}	800	40	134	670
Bottom water					
pH	–	8.0	8.0	8.0	8.0
$[O_2]$	mmol l^{-1}	0.36	0.36	0.36	0.36
$[NO_3^-]$	mmol l^{-1}	0.21	0.21	0.21	0.21
$[Mn^{2+}]$	μmol l^{-1}	0	0	0	0
$[Fe^{2+}]$	μmol l^{-1}	0	0	0	0
$[SO_4^{2-}]$	mmol l^{-1}	0.67	0.67	0.67	0.67
Alkalinity	$mmol_c$ l^{-1}	3.8	3.8	3.8	3.8
$[NH_4^+]$	mmol l^{-1}	0.2	0.1	0.2	0.2
$[CH_4]$	mmol l^{-1}	0	0	0	0

pers. comm.). It should be taken into account that in coastal and freshwater systems, sediment mixing rates may be overestimated using this relationship, especially at high deposition rates. It is important to notice that the measured pore-water profiles can be reproduced satisfactorily without taking additional physical mixing of the solid phase into account. This apparently negligible influence of physical mixing may reflect the relatively low surface area of open water (minimal wave impact) and low current velocities ($<$0.1 m s^{-1}) in the study area. Although irrigation may significantly lower pore water concentrations of solutes, even at very low abundance (Aller 1980), in this study measured concentration profiles can be reproduced satisfactorily without including the effects of irrigation.

Because the sediments at the four locations have a similar origin (river Meuse suspended matter), spatial variability in intrinsic properties of sedimentary phases is neglected. Most chemical and kinetic constants are taken from Wang and Van Cappellen (1996). The limiting concentration for sulphate reduction was set to 0.03 mmol l^{-1} SO_4^{2-}, based on experimental

results of Lovley and Klug (1986) in freshwater sediments. The other limiting values (20 μmol l^{-1} O_2, 2 μmol l^{-1} NO_3^-, 16 μmol g^{-1} MnO_2 and 65 μmol g^{-1} $Fe(OH)_3$) are from Wang and Van Cappellen (1996).

Results and discussion

Bottom-water characteristics

The characteristics of the bottom water are given in Table 1. Most parameter values fall into a narrow range. Relatively large variation in O_2 concentrations and pH may be explained by increased phytoplankton activity during daytime (sampling took place in the productive period). As input to the model the mean values are used, although we recognise the effects of diurnal variation, which may potentially effect benthic primary production in the uppermost millimetres of the sediment. Because bottom water concentrations used as boundary conditions in the model were measured 0.5 m above the sediment surface, these might in certain cases not reflect the actual concentrations at the sediment-water interface. Molar C/N ratios of the suspended matter are in the range 6.8–7.8, which are values typical of planktonic biomass (Tyson 1995).

Sediment characteristics

The top 10 cm of the sediments are characterised by an olive brown layer near the sediment-water interface with a thickness of a few millimetres, underlain by an olive black layer. At location B the olive black layer transforms into a black layer at a depth of 7–8 cm, which extends throughout the core. Absence of a well developed reddish-brown layer may point to limited penetration of oxygen into the sediment and anaerobic conditions close to the sediment-water interface. The observed variation in sediment colour can be interpreted as a change in the predominance from ferric oxyhydroxides to ferrous monosulphides. Characteristics of the sampled sediment cores are given in Table 3. The relatively low standard deviations imply that solid phase levels of OrgC, $CaCO_3$, Fe, Mn, and Al are more or less constant with depth.

Pore-water profiles of redox-sensitive ions are strongly affected by the degradability of the OM. An indication of the degradability and, hence, the extent of mineralisation is given by the C/N ratio. Molar C_{org}/N_{tot} ratios in the top 7 cm of the sediment are on the order of 12.5 ± 0.4 at location A, 13.6 ± 0.9 at location B, 12.4 ± 0.3 at location C and 12.4 ± 0.5 at location D. The C/N ratio of the OM in the suspended matter in the study area (mean ratio of 7.2) is significantly lower than in the sediments. Although this may indicate

Table 3. Characteristics of the sediment cores sampled in June 1996 (weighted averages and standard deviation are given).

	Depth (cm)	OrgC	$CaCO_3$	Al (%)	Fe	Mn
A	0–7	5.6 ± 0.2	9.8 ± 0.3	5.7 ± 0.2	4.4 ± 0.2	0.13 ± 0.01
B	0–7	3.6 ± 0.4	10.4 ± 0.9	3.8 ± 0.4	2.7 ± 0.5	0.08 ± 0.01
C	0–7	5.1 ± 0.3	10.3 ± 0.8	4.9 ± 0.1	3.8 ± 0.1	0.12 ± 0.01
D	0–7	4.9 ± 0.3	10.2 ± 0.4	4.8 ± 0.1	3.9 ± 0.1	0.12 ± 0.01

active biodegradation in the upper centimetres of the sediment, differences in C/N ratios between sediment and suspended matter may also be due to a seasonality due to algal biomass in the water column (Koelmans 1998).

Pore-water profiles

Measured and modelled pore-water profiles are shown in Figures 2 to 5 (note the different scales in the figures). Concentrations in the bottom water are plotted at zero depth. At all locations anaerobic conditions are present directly below the sediment-water interface. Pore-water pH decreases from 8.0 near the sediment-water interface to 7.0–7.5 in the deeper sediment due to production of CO_2. As can be seen in the figures, STEADYSED1 overpredicts the decrease in pH in the sediments studied. This is because the current version of the model does not include $CaCO_3$(s) as a species. The sediments studied have $CaCO_3$ contents in the range 7.0–12.7% at all depths. Thus, it is likely that $CaCO_3$ dissolution buffers a pH decrease in the sediment (Boudreau 1987; Wang & Van Cappellen 1996). Alkalinity increases with depth at all locations, but significant differences in the maximum values reached within 10 cm below the sediment-water interface are measured. In the sediments studied, the production of alkalinity is not only affected by OM degradation and secondary redox reactions, but also significantly by dissolution of $CaCO_3$. In Figures 2 to 5, the modelled curves fit well to those alkalinity profiles which have been corrected for the effect of alkalinity production by $CaCO_3$ dissolution. This alkalinity production is calculated from measured Ca^{2+} pore-water concentrations ($\Delta Alk = 2 \cdot \Delta[Ca^{2+}]$).

Production of ammonium results from the degradation of N-bearing OM substrates (e.g. amino acids) and is, therefore, used as a measure for the overall OM degradation rate. Pore-water ammonium profiles show a typical increase with depth. The slope of the curves decreases with depth indicating a decrease in the OM degradation rate. The maximum concentration of the ammonium profile increases in the order $B < C < A \approx D$ (Figures 2 to

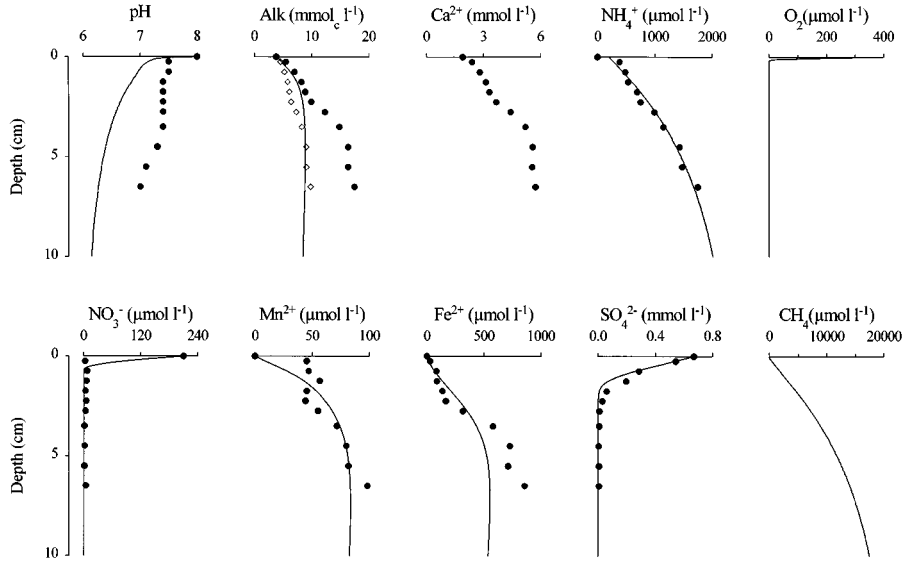

Figure 2. Measured concentrations in the pore water (solid dots) and modelled concentration profiles (lines) at location A (open diamonds represent corrected alkalinity).

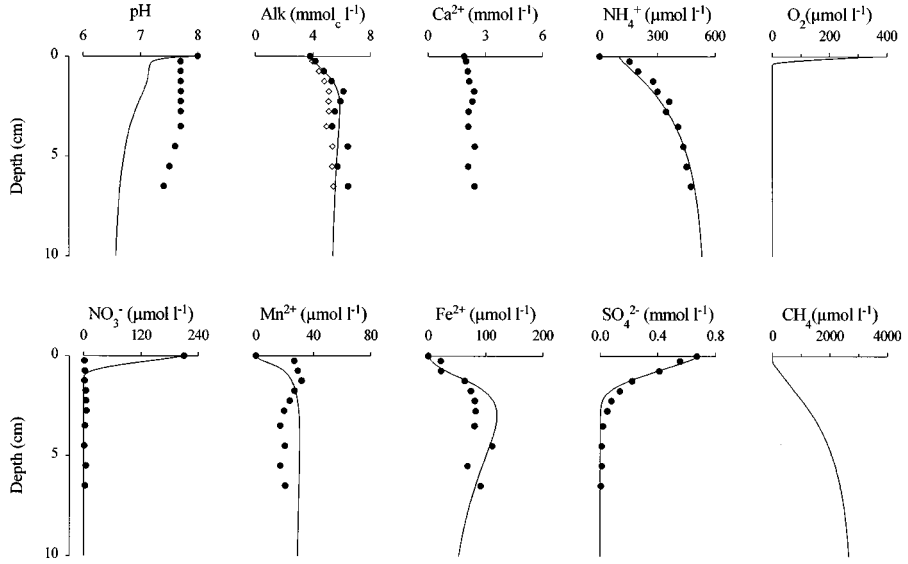

Figure 3. Measured concentrations in the pore water (solid dots) and modelled concentration profiles (lines) at location B (open diamonds represent corrected alkalinity).

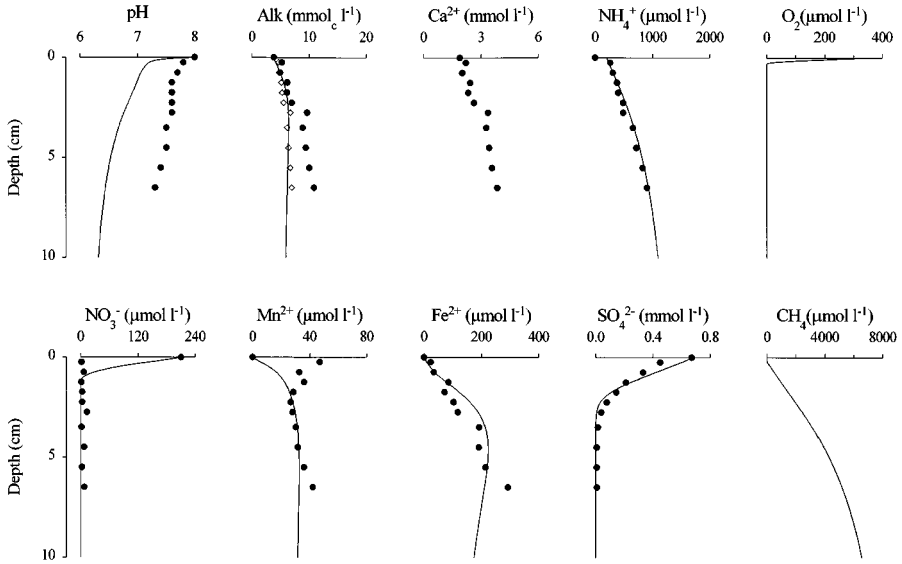

Figure 4. Measured concentrations in the pore water (solid dots) and modelled concentration profiles (lines) at location C (open diamonds represent corrected alkalinity).

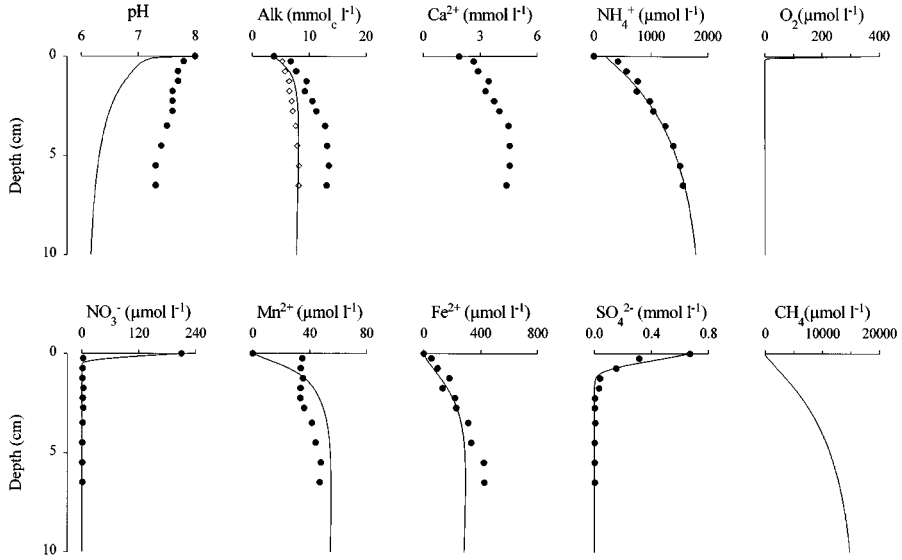

Figure 5. Measured concentrations in the pore water (solid dots) and modelled concentration profiles (lines) at location D (open diamonds represent corrected alkalinity).

Table 4. Depth-integrated rates of OM degradation within the top 10 cm of the sampled sediment cores. The percentage of each pathway to the total OM degradation rate is also shown.

Pathway	A	B	C	D	A	B	C	D
	(μmol cm^{-2} yr^{-1})				(%)			
O_2	90	52	39	122	2.9	11.5	5.0	3.5
NO_3	315	84	125	360	10.1	18.5	16.0	10.4
Mn(IV)	3	<1	<1	4	0.1	<0.1	<0.1	0.1
Fe(III)	212	19	38	177	6.8	4.2	4.9	5.1
SO_4	390	102	140	462	12.5	22.5	17.9	13.3
Methanogenesis	2117	196	439	2338	67.7	43.3	56.2	67.5
Total	3127	453	781	3463				

5), indicating variation in the degradation rate of OM and in transport rates (mixing and accumulation). Slow transport and most degradation at depth in the sediment favour high concentrations of ammonium. The expected variation in OM degradation rates is in keeping with the model results. In Table 4 the calculated values for OM degradation rates at the sediment-water interface and depth-attenuation coefficients (coefficients for the first-order rate of change of organic matter degradation with depth) for each location are given.

The model simulations can be used to compare the importance of reactions controlling the pore-water concentrations of redox-sensitive ions in the sediment cores. Although oxygen-concentration profiles were not actually measured, the model results confirm that aerobic conditions are limited to the upper millimetres of the sediment cores (2 mm at location A and D, 4 mm at location C, and 5 mm at location B), as inferred from the absence of a well developed reddish-brown surface layer and the distribution of redox-sensitive pore-water species. Oxygen consumption is due to aerobic respiration in addition to oxidation of reduced solid-phase (adsorbed Fe(II), adsorbed Mn(II), and FeS) and pore-water constituents (Fe^{2+}, Mn^{2+}, NH_4^+, H_2S, HS^-, and CH_4). Therefore, presence of oxygen in the top few millimetres of the sediment may significantly decrease the flux of reduced pore-water constituents to the bottom water. Calculations with STEADYSED1 predict that in the studied sediments oxygen reduction takes place mainly as a result of oxidation of reduced pore-water constituents. Aerobic degradation of OM only accounts for a relatively small amount of total oxygen reduction (6.6% at location A, 16.9% at location B, 8.1% at location C, and 9.2% at location D). Oxidation

of upward diffusing methane is the main oxygen-consuming process (89% of total oxygen consumption at location A, 34% at location B, 61% at location C, and 88% at location D).

Measured profiles suggest that nitrate is completely reduced within 1 cm below the sediment-water interface. This agrees fairly well with the model results given the fact that the measurements may be somewhat unreliable, because nitrate in nonacidified pore water is sensitive to reduction during storage.

Table 4 shows that the amount of microbial Mn(IV) reduction is negligible compared to the other respiratory pathways in the sediments studied. The shape of the Mn^{2+} pore-water profiles and the asymptotic values are comparable at all locations. Calculations of the saturation state with MINTEQ-A2 (U.S. EPA 1991) show that the anoxic pore waters are saturated with respect to rhodochrosite ($MnCO_3$) below a depth of 2 cm. Thus, $MnCO_3$ may potentially control the pore-water concentrations of Mn^{2+} in these sediments. The sharp increase in dissolved Mn^{2+}, observed in the top 2 cm of cores B, C, and D, cannot be reproduced satisfactorily with STEADYSED1. This may be related to e.g. the presence of a diffusive boundary layer. Vertical separation between pore-water build-up of Mn^{2+} and Fe^{2+} may be caused primarily by oxidation of dissolved Fe^{2+} by MnO_2 (Postma 1985; Wang & Van Cappellen 1996). Calculations suggest that this is the main pathway of Mn reduction in the studied sediments, as it accounts for more than 90% of all Mn(IV) reduction.

Microbial Fe(III) reduction accounts for less than 10% of total degradation of OM in the studied sediments (Table 4). The depth at which the vertical colour transition is observed agrees well with the depth below which Fe^{2+} is present in the pore water. Significant differences are observed in Fe^{2+} concentrations between locations. The gradual increase in pore-water Fe^{2+} with depth may be explained by slow rates of dissolution of Fe(III)-(hydr)oxides and formation of Fe(II) solid phases (Postma 1993; Wersin et al. 1991). However, STEADYSED1 only includes reactive $Fe(OH)_3$ as a Fe-(hydr)oxide species, which may be an oversimplification. FeS was chosen as the only reduced Fe-sulphur species in the model, because FeS generally controls pore-water Fe concentrations in sulphidic freshwater sediments, rather than the thermodynamically more stable pyrite (Boudreau & Canfield 1993). Because there is an excess of Fe^{2+} liberation over HS^- production, siderite ($FeCO_3$) as well as FeS control pore-water Fe^{2+} concentrations in the anoxic layer.

Respiratory sulphate reduction ideally takes place when all other electron acceptors are exhausted, but in the sediments studied significant overlap occurs between the zones of microbial Fe(III) reduction and sulphate reduc-

tion (Figure 6), as will be discussed later. The pore-water sulphate profiles show a rapid decrease to zero concentration within 4 cm at all locations. The model calculations indicate that a small amount (0.5–2.2%) of total sulphate reduction is due to the oxidation of upward-diffusing methane.

In the freshwater sediments studied, the supply of external oxidising agents, especially nitrate and sulphate, is limited and methanogenesis is the dominant process of OM degradation beyond 3 cm below the sediment-water interface at all locations (Figure 6). Calculated concentration profiles (Figures 2 to 5) show that methane is effectively oxidised in the aerobic layer at the sediment-water interface, where methane concentrations are close to zero. In addition, methane diffusing upwards may become a source of carbon for sulphate-reducing bacteria at the sulphate/methane interface (Devol 1983; Iversen & Jörgensen 1985). Calculations show that the amount of methane oxidised by oxygen is much larger (100–500 times) than the amount oxidised by sulphate. It should be noticed that in all cores studied the methane concentrations in the pore water exceed the solubility limit (approximately 1600 μmol l^{-1} CH_4 at 1 atmosphere). As a consequence of methane accumulation in the pore water, concentration gradients increase and CH_4 oxidation rates are higher than they would be when the solubility limit would have been included. Methane release through bubbles results in limited oxidation, because the zone of methane oxidation is passed by (Martens & Klump 1980; Martens et al. 1998). Because methane ebullition is not included in the model, the contribution of methane oxidation to oxygen demand may consequently be overestimated. Hence, the contribution of the other oxidants is underestimated, and the results in Table 4 may only be indicative.

Organic matter degradation pathways

By fitting STEADYSED1 to the measured pore-water concentration profiles, the rate distributions of the OM degradation pathways are calculated (Figure 6). The calculated depth distributions of microbially-mediated electron transfer reactions within the sediment are roughly in accordance with their corresponding redox potentials (Stumm & Morgan 1996) and correspond to that observed in marine systems (Froelich et al. 1979). However, the model predicts considerable vertical overlap between the degradation pathways. This overlap reflects the high mixing intensities of the sediments in combination with limiting values of the respiratory electron acceptors (Wang & Van Cappellen 1996). Additionally, in a one-dimensional modelling approach, as used in this study, considerable overlap may result from lateral heterogeneity of the sediment, as proposed by Brandes and Devol (1995) and Wang and Van Cappellen (1996) and the presence of a wide range of mineral reactivities (Postma & Jakobsen 1996).

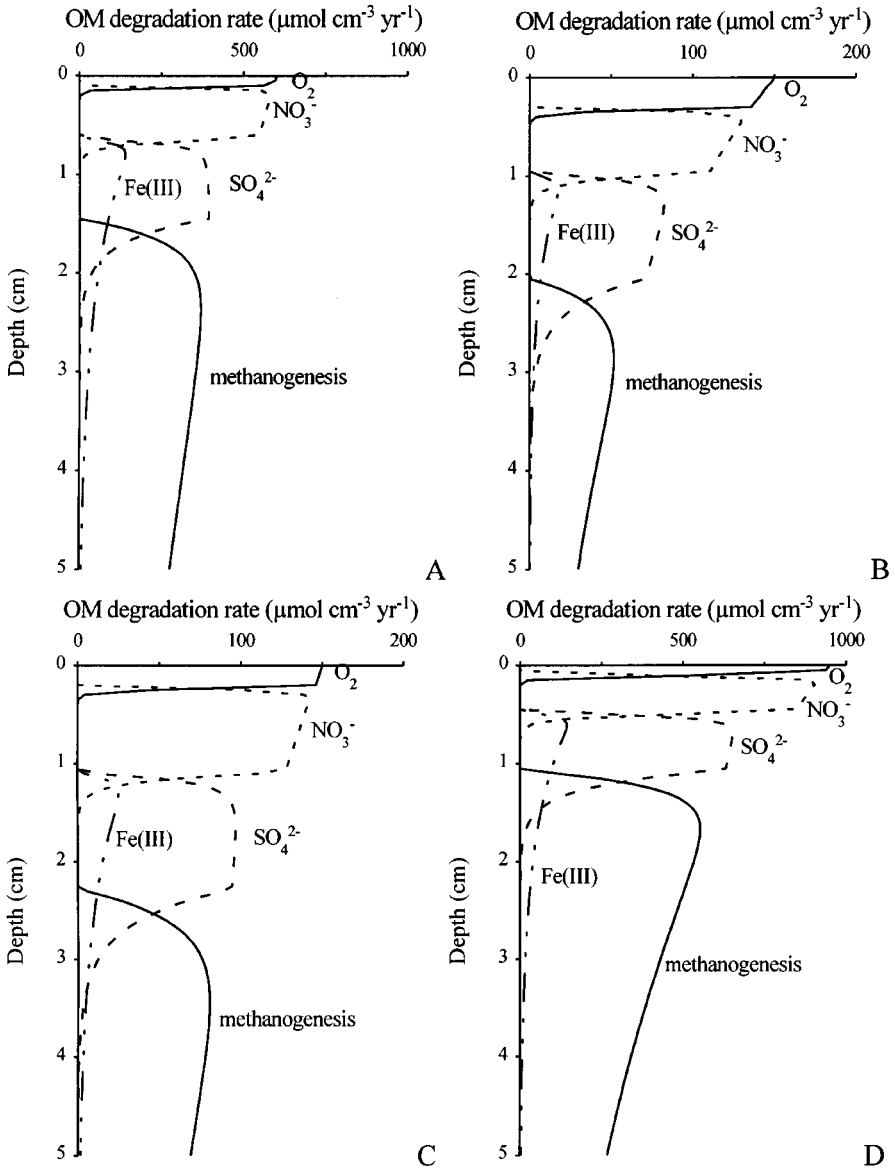

Figure 6. OM degradation rates of the relevant electron acceptors in the top 5 cm of the sediment at the four locations studied. OM degradation rates coupled to Mn(IV) reduction are not shown, because the role of dissimilatory Mn(IV) reduction seems negligible compared to the other degradation pathways (Table 4). Note the different rates on the x-axis.

Depth-integrated rates of OM degradation are given in Table 4. Rates differ between locations, reflecting variations in depositional conditions, primarily the rate of supply of reactive OM. Table 4 clearly shows that methanogenesis is the most important OM degradation process in the studied sediments. The relative importance of methanogenesis increases with overall rate of OM degradation (on the order B < C < A ≈ D), although supersaturation of the pore water with respect to methane suggests that OM degradation rates by methanogenesis may be overestimated. The importance of the suboxic pathways decreases with the overall OM degradation rate. The extent of $CaCO_3$ dissolution in the sediments studied, as indicated by the Ca^{2+} pore-water concentration profiles (Figures 2 to 5), increases with integrated rates of O_2 reduction and methanogenesis (Table 4), which are the main producers of CO_2 driving the $CaCO_3$ dissolution reaction. This correlation supports the internal consistency of the predicted integrated rates of O_2 reduction and methanogenesis.

Conclusions

Early diagenetic processes in organic-rich freshwater sediments can be described quantitatively with the general diagenetic reaction/transport model STEADYSED1. The application of this model was successful and shows the generality of this approach, although incorporation of other processes, especially $CaCO_3$ dissolution/precipitation and methane bubble formation and ebullition may improve the application in such sediments. Pore-water profiles can be explained by the degradation of OM and the internal cycling of redox species. The main pathway for OM degradation in the sediments studied is methanogenesis. The other oxidative pathways (O_2, NO_3^-, Mn(IV), Fe(III), and SO_4^{2-} reduction) are limited to the top 3 cm of the sediments. Model results show that oxygen consumption takes place mainly by methane oxidation, and only to a limited extent by aerobic respiration. Oxidation of dissolved Fe^{2+} by MnO_2 seems the main pathway of Mn reduction in the sediments studied. The differences in the pore-water profiles of redox-sensitive ions at the sites studied are mainly the result of large differences in the depth-integrated rates of OM degradation.

Acknowledgement

The authors thank P. Van Cappellen (Georgia Institute of Technology) for his interest in this work and for his useful comments on an earlier version of the manuscript. The manuscript greatly benefited from the suggestions of J.J.

Middelburg on a previous draft. The critical comments of three anonymous reviewers are gratefully acknowledged. The suggestions made by C.H. van der Weijden throughout the research project are appreciated. The assistance of Pieter Kleingeld, Gijs Nobbe and Mark van Alphen during sampling and in the laboratory is greatly appreciated. This project was carried out with the financial support of the Ministry of Transport, Public Works and Water Management, Institute for Inland Water Management and Waste Water Treatment (RIZA).

References

Aller RC (1980) Quantifying solute distributions in the bioturbated zone of marine sediments by defining an average microenvironment. Geochim. Cosmochim. Acta 44: 1955–1965

Berner RA (1980) Early Diagenesis: A Theoretical Approach. Princeton Univ. Press

Boudreau BP (1987) A steady-state diagenetic model for dissolved carbonate species and pH in the porewaters of oxic and suboxic sediments. Geochim. Cosmochim. Acta 51: 1985–1996

Boudreau BP & Canfield DE (1993) A comparison of closed- and open-system models for porewater pH and calcite-saturation state. Geochim. Cosmochim. Acta 57: 317–334

Brandes JA & Devol AH (1995) Simultaneous nitrate and oxygen respiration in coastal sediments: Evidence for discrete diagenesis. J. Mar. Res. 53: 771–797

Calmano W, Hong J & Förstner U (1993) Binding and mobilization of heavy metals in contaminated sediments affected by pH and redox potential. Wat. Sci. Technol. 28: 223–235

Capone DG & Kiene RP (1988) Comparison of microbial dynamics in marine and freshwater sediments: Contrasts in anaerobic carbon catabolism. Limnol. Oceanogr. 33: 725–749

De Lange GJ (1992) Shipboard routine and pressure filtration system for pore water extraction from suboxic sediments. Mar. Geol. 109: 77–81

Devol AH (1983) Methane oxidation rates in the anaerobic sediments of Saanich Inlet. Limnol. Oceanogr. 28: 738–742

Dhakar SP & Burdige DJ (1996) A coupled, non-linear, steady-state model for early diagenetic processes in pelagic sediments. Am. J. Sci. 296: 244–265

Van Eck BTM, Zwolsman JJG & Saeijs HLF (1997) Influence of compartmentalization on the water quality of reservoirs: Lessons learned from the enclosure of the Haringvliet estuary, The Netherlands. In: Dix-neuvième congrès des grands barrages, Volume III (pp 647–669). Commission internationale des grands barrages, Florence, France

Förstner U, Calmano W, Hong J & Kersten M (1994) Effects of redox variations on metal speciation: Implications on sediment quality criteria assessment. In: Special Publication 154 (pp 83–102). The Royal Society of Chemistry, London

Froelich PN, Klinkhammer GP, Bender ML, Luedtke NA, Heath GR, Cullen D, Dauphin P, Hammond D, Hartman B & Maynard V (1979) Early oxidation of organic matter in pelagic sediments of the eastern equatorial Atlantic: Suboxic diagenesis. Geochim. Cosmochim. Acta 43: 1075–1090

Gaillard JF, Jeandel O, Michard G, Nicolas E & Renard D (1986) Interstitial water chemistry of Villefranche Bay sediments: Trace metal diagenesis. Mar. Chem. 18: 233–247

Iversen N & Jörgensen BB (1985) Anaerobic methane oxidation rates at the sulfate-methane transition in marine sediments from Kattegat and Skagerrak (Denmark). Limnol. Oceanogr. 30: 944–955

Koelmans AA (1998) Geochemistry of suspended and settling solids in two freshwater lakes. Hydrobiologia 364: 15–29

Lovley DR & Klug MJ (1986) Model for the distribution of sulfate reduction and methanogenesis in freshwater sediments. Geochim. Cosmochim. Acta 50: 11–18

Martens CS, Albert DB & Alperin MJ (1998) Biogeochemical processes controlling methane in gassy coastal sediments 1. A model coupling organic matter flux to gas production, oxidation and transport. Cont. Shelf. Res. 18: 1741–1770

Martens CS & Klump JV (1980) Biogeochemical cycling in an organic-rich coastal marine basin-1. Methane sediment-water exchange processes. Geochim. Cosmochim. Acta 44: 471–490

Postma D (1985) Concentration of Mn and separation from Fe in sediments-1. Kinetics and stoichiometry of the reaction between birnessite and dissolved Fe(II) at 10 °C. Geochim. Cosmochim. Acta 45: 687–698

Postma D (1993) The reactivity of iron oxides in sediments: A kinetic approach. Geochim. Cosmochim. Acta 57: 5027–5034

Postma D & Jakobsen R (1996) Redox zonation: Equilibrium constraints on the Fe(III)/SO_4-reduction interface. Geochim. Cosmochim. Acta 60: 3169–3175

Rabouille C & Gaillard JF (1991) Toward the EDGE: Early diagenetic global explanation: A model depicting the early diagenesis of organic matter, O_2, NO_3, Mn, and PO_4. Geochim. Cosmochim Acta 55: 2511–2525

Santschi P, Höhener P, Benoit G & Buchholtz-ten Brink M (1990) Chemical processes at the sediment-water interface. Mar. Chem. 30: 269–315

Shaw TJ, Gieskes JM & Jahnke RA (1990) Early diagenesis in differing depositional environments: The response of transition metals in pore water. Geochim. Cosmochim. Acta 54: 1233–1246

Soetaert K, Herman PMJ & Middelburg JJ (1996) A model for early diagenetic processes from the shelf to abyssal depths. Geochim. Cosmochim. Acta 60: 1019–1040

Solorzano L (1969) Determination of ammonia in natural waters by the phenolhypochlorite method. Limnol. Oceanogr. 14: 799–801

Stumm W & Morgan JJ (1996) Aquatic Chemistry, Chemical Equilibria and Rates in Natural Waters. Wiley, New York

Tromp TK, Van Cappellen P & Key RM (1995) A global model for the early diagenesis of organic carbon and organic phosphorus in marine sediments. Geochim. Cosmochim. Acta 59: 1259–1284

Tyson RV (1995) Sedimentary Organic Matter, Organic Facies and Palynofacies. Chapman & Hall, London, U.K.

U.S. Environmental Protection Agency (1991) MINTEQA2/PRODEFA2, a geochemical assessment model for environmental systems: Version 3.0 users manual. USEPA Rep. 600/3-91/021. USEPA, Washington, DC

Van den Berg GA (1998) Geochemical behaviour of heavy metals in a sedimentation area of the rivers Rhine and Meuse. PhD thesis, Utrecht University, The Netherlands

Van Cappellen P & Gaillard JF (1996) Biogeochemical dynamics in aquatic sediments. In: Lichtner PC, Steefel CI & Oelkers EH (Eds) Reactive Transport in Porous Media. Reviews in Mineralogy 34 (pp 335–376). Mineralogical Society of America, Washington, DC

Van Cappellen P & Wang Y (1995) Metal cycling in surface sediments: Modeling the interplay of transport and reaction. In: Allen HE (Ed) Metal Contaminated Aquatic Sediments (pp 21–64). Ann Arbor Press, Chelsea, Michigan

Van Cappellen P & Wang Y (1996) Cycling of iron and manganese in surface sediments: A general theory for the coupled transport and reaction of carbon, oxygen, nitrogen, sulfur, iron and manganese. Am. J. Sci. 296: 197–243

Wang Y & Van Cappellen P (1996) A multicomponent reactive transport model of early diagenesis: Application to redox cycling in coastal marine sediments. Geochim. Cosmochim. Acta 60: 2993–3014

Wersin P, Höhener P, Giovanoli R & Stumm W (1991) Early diagenetic influences on iron transformations in a freshwater lake sediment. Chem. Geol. 90: 233–252